American Mineralogist, Volume 76, pages 313–331, 1991

Static lattice energy minimization and lattice dynamics calculations on aluminosilicate minerals

Bjorn Winkler, Martin T. Dove
Department of Earth Sciences, University of Cambridge, Downing Street, Cambridge CB2 3EQ, United Kingdom
Maurice Leslie
Daresbury Laboratory, Warrington, Cheshire WA4 4AD, United Kingdom

Abstract

Lattice energy minimization and lattice dynamics calculations for the minerals andalusite, sillimanite, kyanite, diopside, cordierite, gehlenite, leucite, orthozoisite, grossular, and pyrope are compared with experimental data and previous calculations. The potential models used in this study included bond-bending interactions, short-range Born-Mayer forces, effective dispersive interactions, long-range Coulomb interactions, and harmonic core-shell interactions for the O ions. Parameters for the potential models were generally taken from the literature, but the core-shell force constant was modified to give better agreement with experimental data for refractive indices. It was necessary to include bond-bending interactions for Al-O polyhedra with coordination numbers even larger than four. A method for describing effective potentials with Al-Si disorder and solid-solution is presented. Modified Morse and Buckingham potentials were used to model O-H bonds. Relaxed energy-minimum structures were calculated, allowing cell parameters to change and treating atomic cores and shells as independent entities within the adiabatic approximation. Calculated phonon frequencies for the relaxed structures were used to construct thermodynamic functions. Elastic and dielectric constants were also calculated. Comparisons between calculated structures and other properties with experimental data have shown that the model is genuinely transferable and gives reasonable predictions of crystallographic, physical, and thermodynamic properties. Detailed analysis gives a measure of the reliability of the model.

Introduction

The recent interest in static lattice energy calculations (SLEC) and harmonic lattice dynamics calculations (HLDC) for aluminosilicate minerals is partly motivated by the insights such calculations give about interatomic forces. An immediate application of reliable SLEC and HLDC is for equilibrium thermodynamics, where such models could provide data, e.g., on solid solutions, which are tedious to obtain experimentally. It is hoped that these calculations can provide information about thermodynamic and physical properties of minerals under extreme conditions of pressure or temperature that are not readily attainable in the laboratory. Reliable HLDC models will also permit the interpretation of complex spectroscopic data (e.g., Raman, infrared, or inelastic neutron scattering data). Furthermore, thermodynamic properties can be calculated from SLEC and HLDC, and these relations can be used to provide valuable insights into phase transition behavior. Other applications include studies of defect energies and transport mechanisms. Finally, as molecular dynamics simulations are used increasingly to study phase transitions in minerals, the need for tested reliable potentials becomes more urgent.

The first aim of this study is to assess the transferability of previously published potentials for modeling the structures of complex minerals using SLEC. We have selected a number of structures that we consider to have features that provide balanced tests. The Al_2SiO_5 polymorphs, andalusite, sillimanite, and kyanite, each have one six-coordinated Al and one four-coordinated Si, but differ in the coordination number of the second Al, which is four in sillimanite, five in andalusite, and six in kyanite. Diopside ($CaMgSi_2O_6$) has a complex chain structure with irregular Ca coordination. Gehlenite ($Ca_2Al_2SiO_7$) has a layer structure with Al-Si disorder and significantly different bond lengths within the Ca coordination polyhedron. Cordierite ($Mg_2Si_5Al_4O_{18}$) is by some definitions a framework structure with an Al-Si order-disorder phase transition that is accompanied by a small spontaneous strain. Leucite ($KAlSi_2O_6$) has a true framework structure. Experiments suggest that there is no long-range Al-Si order at all temperatures. Leucite also undergoes a structural phase transition that is accompanied by a spontaneous strain. The garnets pyrope ($Mg_3Al_2Si_3O_{12}$) and grossular ($Ca_3Al_2Si_3O_{12}$) are orthosilicates in which all the corners of the SiO_4 tetrahedra and the AlO_6 octahedra are shared, leading to nearly regular triangular dodecahedra

0003–004X/91/0304–0313$02.00

containing the Ca or Mg cations. The complex structure of zoisite [$Ca_2Al_3Si_3(OH)O_{12}$] contains Si_2O_7 and SiO_4 groups as well as chains of AlO_6 octahedra that are partly linked by H bonds. Such a wide range of structures provides a stringent test for a single set of transferable potential parameters.

The second aim of this study is to demonstrate that these same transferable potential parameters can also reproduce vibrational properties using HLDC. The third aim is to show that reliable thermodynamic functions for complex minerals can be obtained from HLDC. This emphasizes the link between microscopic interactions and macroscopic properties.

The development of transferable model potentials for minerals is vital if computer modeling techniques are to be used as predictive methods. As Dove (1989) has pointed out, there is no overall consensus on the forms of the potentials to be used and on how numerical values of parameters in the respective models should be obtained. The potentials that are currently available have been derived by a number of different methods, e.g., ab initio quantum mechanical calculations (Lasaga and Gibbs, 1987), modified electron gas (MEG) calculations (Post and Burnham, 1986), and empirical fitting procedures (Abbott et al., 1989a, 1989b; Collins and Catlow, 1990). A promising empirical approach has been suggested by the very successful modeling of quartz (Sanders et al., 1984), forsterite (Price and Parker, 1988), diopside (Dove, 1989), micas (Collins and Catlow, 1990), and zeolites (Jackson and Catlow, 1988) using a model that includes three-body bond-bending interactions and core-shell forces. We have therefore chosen to work exclusively with this model in this study, employing previously published potential parameters where appropriate.

The outline of this paper is as follows. In the next section we summarize the thermodynamic relations used in this paper. Then we discuss the potential models in detail. Following that, we present the results of our SLEC and HLDC for each material studied. Our aim is to present a brief comparison between the calculated and observed structures for each example and to give a more detailed analysis of some of the more interesting features of each calculation. This reflects the fact that the best tests of any model are the predictions of subtle effects (such as may be associated with phase transitions). These are a greater challenge for the modeler than simply the predictions of structures. Finally we present a general analysis of the results common to all systems, highlighting the transferable aspects of the potential model.

The thermodynamic basis

In the quasi-harmonic approximation, a crystal's internal energy, E, can be described as a sum of the static lattice energy, ϕ, and the vibrational energy, E_{vib}:

$$E = \varphi + E_{vib}. \tag{1}$$

The static lattice energy, φ, is the sum over all interatomic interactions. The vibrational energy, E_{vib}, is given by

$$E_{vib} = \sum_{j,\mathbf{k}} \hbar\omega_j(\mathbf{k})\left[\frac{1}{2} + n(\omega, T)\right] \tag{2}$$

where $\omega_j(\mathbf{k})$ denotes the frequency of the jth mode at wavevector $\mathbf{k}$. The term, $n(\omega, T)$, is the Bose-Einstein distribution:

$$n(\omega, T) = \left\{\exp\left[\frac{\hbar\omega}{k_B T}\right] - 1\right\}^{-1}. \tag{3}$$

Since $n(\omega, T)$ is independent of wavevector and mode number, the sum in Equation 2 can be replaced by an integral over the density of states, $g(\omega)$:

$$E_{vib} = \int \hbar\omega\left[\frac{1}{2} + n(\omega, T)\right] g(\omega)\mathrm{d}\omega. \tag{4}$$

Note that we are assuming infinite perfect crystals throughout this study. The only quantity in Equation 4 that is dependent on the actual structure is $g(\omega)$. The density of states is a rather demanding quantity to calculate from a computational viewpoint. Calculations involving a fine grid over the Brillouin zone are impractical; however, calculations using only a single point (e.g., the Γ or $\mathbf{k} = 0$ point) are prone to errors caused by the neglect of phonon dispersion. This point is discussed in more detail by Price and Parker (1988). The use of representative points for cubic lattices has been suggested (Baldereschi, 1973), but such points are also prone to errors in the calculated $g(\omega)$, particularly at low frequencies. We used the Baldereschi point (1/6, 1/6, 1/2) for the I-centered cubic garnets. For all other systems we have made the pragmatic choice of constructing $g(\omega)$ from HLDC performed at the Γ point and at points on the faces of the Brillouin zone. By doing this, we hope that the effects of frequency dispersions are adequately taken into account, albeit in a coarse way. However, since most of the modes only show weak dispersion, the only significant source of error will arise from the contribution of the acoustic models to $g(\omega)$. This is only a problem for the calculation of thermodynamic properties at low temperature ($T < 50$ K), which is lower than the range of interest of most mineral scientists.

The heat capacity at constant volume, C_V, can be calculated readily from the internal energy:

$$C_V = \left(\frac{\mathrm{d}E}{\mathrm{d}T}\right)_V = k_B \int \left[\frac{\hbar\omega n(\omega, T)}{k_B T}\right]^2 \exp\left(\frac{\hbar\omega}{k_B T}\right) g(\omega)\mathrm{d}\omega. \tag{5}$$

The heat capacity at constant pressure, C_P, is the experimentally determined quality. It can be derived from C_V using the isotropic thermal expansion coefficient, α, and the isotropic compressibility modulus, β:

$$C_P = C_V + TV_0\alpha^2\beta^{-1} \tag{6}$$

where V_0 is the molar volume at 298 K and 1 bar. In our calculations of the heat capacities, we used experimental values for the coefficients α and β. They could in fact have been calculated from a lattice dynamics calculation (Price and Parker, 1988) within the quasi-harmonic approximation using the Grüneisen approach. However, such calculations are rather lengthy, and, for the purposes of this paper, the effort expended on these calculations would not be justified. Instead, when we compared calculated and measured heat capacities, it should be considered that we really compared C_V rather than C_P. In any case, the differences between these quantities are never large at the temperatures we considered. It should be stressed that we used thermodynamic quantities in this paper, not to test the basic model, but to show that our model is capable of giving thermodynamic information for many cases of interest.

The Helmholtz free energy, F, for a vibrating crystal has been given by Born and Huang (1954):

$$F = \varphi - \int \left\{\frac{1}{2}\mathrm{h}\omega + k_B T \ln[n(\omega, T)]\right\} g(\omega)\, \mathrm{d}\omega. \quad (7)$$

The entropy, S, is then

$$S = -\frac{\partial F}{\partial T} = k_B \int \left\{\ln[n(\omega, T)] + \frac{\mathrm{h}\omega}{T}[n(\omega, T) + 1]\right\} \cdot g(\omega)\, \mathrm{d}\omega. \quad (8)$$

Phase boundaries can be determined by the Clausius-Clapeyron equation. We neglect the pressure dependence of the entropy term and write

$$\frac{\mathrm{d}P}{\mathrm{d}T} = \frac{\Delta S(T)}{\Delta V(P, T)}. \quad (9)$$

Implicit in the applications of these equations is the assumption that $g(\omega)$ is independent of T and P. This implies the neglect of phonon frequency renormalization due to anharmonic effects. Although experimentally it is known that the individual phonon frequencies do vary significantly with T and P, the overall effect on $g(\omega)$ is much smaller. Moreover, for calculations of phase boundaries, the important aspects are the differences between $g(\omega)$ of different phases, and these are expected to be even less sensitive to changes in T and P.

The interatomic potential model

The basic interatomic potential model has been described by Catlow (1988). O ions are modeled using the core-shell model, where a massless shell is linked to the core by ideal harmonic interactions of the form

$$\varphi(d) = \frac{1}{2} K d^2 \quad (10)$$

where d is the separation between centers of core and shell. Polarization effects are therefore taken into account, enabling the high frequency dielectric constant to be correctly evaluated.

Pair interactions between neighboring O shells are modeled using a Buckingham potential:

$$\varphi(r) = -\frac{A}{r^6} + B \exp\left(-\frac{r}{\rho}\right) \quad (11)$$

where r is the interionic distance. The same potential is used for Si-O interactions, where the interaction involves the O shell and a rigid Si ion.

Al-O pair interactions are modeled using a Born-Mayer potential:

$$\varphi(r) = B \exp\left(-\frac{r}{\rho}\right) \quad (12)$$

where the interaction is between a rigid Al ion and the O shell. The same potential was used for Al in all coordinations. All other cation-O pair interactions are modeled similarly. Electrostatic Coulomb interactions are evaluated using formal charges. Covalent effects are simulated using three-body bond-bending interactions. They have the form

$$\varphi(\theta) = \frac{1}{2} k(\theta - \theta_0)^2 \quad (13)$$

where θ is the O-Si-O or O-Al-O bond angle, θ_0 being the respective angle in an undistorted polyhedron.

The values for the parameters in Equations 10–13 are given in Table 1. The values for Si-O and O-O interactions have been taken from the work of Sanders et al. (1984) on quartz. Following Jackson and Catlow (1988), we have taken the values for Al-O interactions from Catlow et al. (1982) and have used these values for all coordinations. The value for k in Equation 13 was considered to be the same for all Al coordinations and equal to the value for O-Si-O interactions. Only the value of θ_0 was modified for different coordinations. We have modified the value of K in Equation 10. Parameters for Ca-O and K-O interactions have been taken from the MEG calculations of Post and Burnham (1986). The parameters for the Mg-O interaction could have been taken from the same source; instead, we used the same values used by Price and Parker (1988) and Dove (1989). Dove (1989) has pointed out that these potentials give similar results.

O-H potentials were adapted by us from the work of Collins and Catlow (1990), who used a modified Morse potential of the form

$$\varphi(r) = \epsilon\{1.0 - \exp[-\alpha(r - \mu)]\}^2 - \epsilon - \varphi_{\text{Coulomb}}. \quad (14)$$

The parameters for Equation 14 are also given in Table 1.

The SLEC and HLDC were performed using the programs THB_REL and THB_PHON, respectively, which explicitly include the interactions described above. These programs evaluate the Coulomb contribution to the lattice energy using the Ewald method. THB_REL uses a

TABLE 1. Potential parameters used in this work[1]

	A [eV]	ρ [Å]	C [eV Å^{-6}]	Ref[3,4]
Short-range interactions: Born-Mayer or Buckingham type between cation cores and O shells[2]				
$Si^{4+}-O^{2-}$	1283.9073	0.3205	10.6616	[1]
$Si^{4+}-O^{1.426-}$	999.98	0.3012	0.0	[2]
$Al^{3+}-O^{2-}$	1460.3	0.29912	0.0	[3]
$K^{+}-O^{2-}$	65269.71	0.2130	0.0	[4]
$Ca^{2+}-O^{2-}$	6958.3	0.2516	0.0	[4]
$Mg^{2+}-O^{2-}$	1428.5	0.2945	0.0	[5]
$O^{2-}-O^{2-}$	22764.0	0.149	27.88	[1]
$H^{+}-O^{-2}$	311.97	0.25	0.0	[6]
Short-range interactions: modified Morse type between cores[5]	ϵ [eV]	α [Å^{-1}]	μ [Å]	
$H^{0.426+}-O^{1.426-}$	7.0525	2.1986	0.9485	[2]
Shell-core interaction between O shell and O core[6]	K [eV Å^{-2}]			
$O_{Core}^{-0.86902}-O_{Shell}^{2.86902}$	60.00			
Three-body bond-bending interactions[7]	k [eVrad^{-2}]	θ_0 [°]		
$O^{2-}-Si^{4+}-O^{2-}$	2.09724	109.47		[1]
$O^{2-}-Al^{3+}-O^{2-}$	2.09724	90, 95, 109.47[8]		

[1] eV units are quoted as these are the units used by THB_REL. 1 eV = 96.484 kJ mol^{-1}.

[2] Defined by Equations 11–12.

[3] The charges used are given in the ion description, in units of the electron charge.

[4] The references cited are: [1] Sanders et al. (1984), [2] Collins and Catlow (1990), [3] Catlow et al., (1982), [4] Post and Burnham (1986), [5] Price and Parker (1988), [6] Abbott et al., (1989a, 1989b).

[5] Defined by Equation 14.

[6] Defined by Equation 10.

[7] Defined by Equation 11.

[8] The three values given for the three-body O-Al-O bond-bending interactions refer to octahedral, irregular five-, and tetrahedral coordination, respectively.

standard Newton minimization technique for the lattice relaxation. THB_REL does not use symmetry, and the minimizations are performed assuming triclinic ($P1$) symmetry. Thus, if the relaxed structure contains a higher symmetry (e.g., equal cell lengths or atoms in a special position) the symmetric structure represents a global minimum and not a minimum under any constraints. The only condition imposed is the number of atoms in the unit cell and, in practice, the topology of the structure. In all cases where a structure with a symmetry higher than $P1$ was obtained, we report only the symmetrically independent parameter values rather than duplicate equivalent quantities. We found that, in these cases, cell lengths were calculated to be equal with precision far greater than that given in the tables, and that deviations from special angles, 90° or 120°, did not appear in the first ten digits. Degenerate phonon frequencies deviated by less than 10^{-5}%.

THB_REL automatically calculates the complete elastic constant tensor. The components are evaluated in the program from the strain derivatives of a series expansion of the lattice energy in terms of lattice and internal strains. The terms in which the lattice strains and the internal strains are coupled automatically give the relaxation of the structure under strain, ensuring that all the contributions to the elastic constants are correctly evaluated.

Some general observations

We found that some complex structures containing Al coordinated by more than four O atoms could not be successfully relaxed without taking the covalent bond-bending effects into account. We found that our best model for six-coordinated Al includes O-Al-O three-body bond-bending interactions for all O-O distances less than 3 Å with $\theta_0 = 90°$ in Equation 13, whereas the parameter k in Equation 13 is the same as for tetrahedrally coordinated Al and Si (Table 1). We found that, in the case of five-coordinated Al in andalusite, the best model included the bond-bending term with $\theta_0 = 95°$. We should remind the reader that identical Born-Mayer Al-O pair interactions were used for all coordinations.

When using a force constant, $K = 74$ eV Å^{-2}, for the core-shell interaction in Equation 10 (Sanders et al., 1984), we found that our calculations of the high-frequency dielectric constant gave values that were generally approximately 20% too low when compared with experimental data. For example, the average observed values for andalusite and kyanite are 2.7 and 3.0, respectively (values have been taken as the squares of the average refractive indices given by Deer et al., 1966), and the corresponding calculated values are 2.2 and 2.5. A decrease of the value of this force constant to 60 eV Å^{-2} gave improved results, not only for the high-frequency dielectric constants (new values for andalusite and kyanite are 2.54 and 2.88), but also for most of the basic structures and the elastic constants, although for some structures the changes were small. We note that the introduction of a further value for a potential parameter might be confusing, but we believe that our results justify this. However, our new value is not an optimized value and, therefore, should be improved upon in any future attempt to develop the potential model.

A model for Al-Si disorder and solid solutions

In some of the systems we have studied there is site occupancy disorder, such as in disordered Al-Si arrangements or as in a solid solution. In order to model these cases, we have devised a simple recipe to construct effective interactions from the pure interactions as given in Table 1. In our formulation, the fraction of atom type 1 on a site is x, so that the fraction of type 2 is $(1 - x)$. The effective charge is thus

$$Q_{\text{eff}} = xQ_1 + (1 - x)Q_2. \tag{15}$$

The effective A parameter for the r^{-6} interaction in the Buckingham potential of Equation 11 is similarly given by

$$A_{\text{eff}} = xA_1 + (1 - x)A_2. \tag{16}$$

The effective Born-Mayer coefficients B and r for Equations 11 and 12 were determined by setting the first and

second derivatives of the effective interaction equal to the weighted averages of the derivatives of the component interactions for the observed bond length $r = r_0$:

$$\left(\frac{\partial\varphi_{\text{eff}}}{\partial r}\right)_{r=r_0} = x\left(\frac{\partial\varphi_1}{\partial r}\right)_{r=r_0} + (1-x)\left(\frac{\partial\varphi_2}{\partial r}\right)_{r=r_0} \quad (17)$$

$$\left(\frac{\partial^2\varphi_{\text{eff}}}{\partial r^2}\right)_{r=r_0} = x\left(\frac{\partial^2\varphi_1}{\partial r^2}\right)_{r=r_0} + (1-x)\left(\frac{\partial^2\varphi_2}{\partial r^2}\right)_{r=r_0}. \quad (18)$$

This gives the following relations for ρ_{eff} and B_{eff}:

$$\rho_{\text{eff}} = \frac{x\rho_1^{-1}B_1\exp(-r_0/\rho_1) + (1-x)\rho_2^{-1}B_2\exp(-r_0/\rho_2)}{x\rho_1^{-2}B_1\exp(-r_0/\rho_1) + (1-x)\rho_2^{-2}B_2\exp(-r_0/\rho_2)} \quad (19)$$

$$B_{\text{eff}} = \frac{x\rho_1^{-1}B_1\exp(-r_0/\rho_1) + (1-x)\rho_2^{-1}B_2\exp(-r_0/\rho_2)}{\rho_{\text{eff}}^{-1}\exp(-r_0/\rho_{\text{eff}})}. \quad (20)$$

This formalism can be readily extended for cases involving more than two atom types. It should be noted that although this method should give reliable differentials of the effective potential, and hence for equilibrium structures, it is not expected to give accurate values for the effective energy, since the energy has not been incorporated into the method. However, we will find that this method still gives good results for the energy of mixing in a solid solution.

The Al_2SiO_5 polymorphs

There are three Al_2SiO_5 polymorphs: andalusite (*Pnnm*), sillimanite (*Pbnm*), and kyanite ($P\bar{1}$). In all three structures there are $Z = 4$ formula units per unit cell; for our purposes, the significant difference among the three structures is in the coordination of one of the Al atoms, as described earlier. The structures of the Al_2SiO_5 polymorphs are therefore a good test of transferable Al-O potentials. Moreover, the calculation of the Al_2SiO_5 phase diagram was seen as a test of whether our model could reproduce the relatively small differences in the thermodynamic properties of the polymorphs. This is important for the application of SLEC and HLDC in equilibrium thermodynamics as needed in petrology.

Because of the use of the Al_2SiO_5 polymorphs as petrogenetic indicators, a number of experimental studies have been performed to determine the positions of the univariant reaction boundaries and the triple point of this system. Robie and Hemingway (1984) summarized previously published work and determined the thermodynamic properties of all the polymorphs. Furthermore, they redetermined the Al_2SiO_5 phase diagram (Fig. 1 and Table 2). There are difficulties in determining the reaction boundaries accurately, due to small differences in the respective Gibbs free energies, kinetic problems, and influence of defects and fibrolitization, as discussed by Salje and Werneke (1982a, 1982b) and Salje (1986). To overcome these problems, Salje and Werneke (1982a, 1982b)

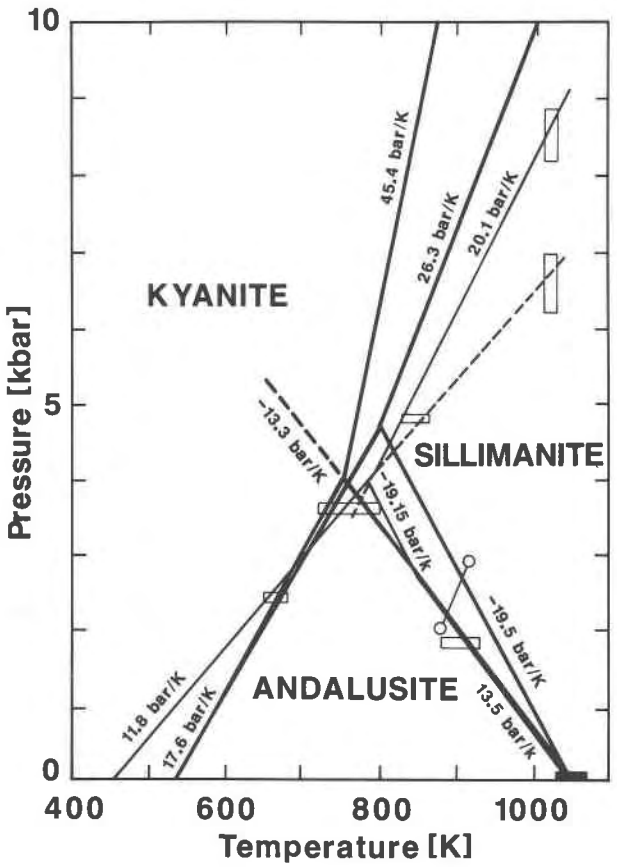

Fig. 1. The phase diagram of Al_2SiO_5. The experimental data (thin lines) are from Robie and Hemingway (1984). The results from our calculations (model 1 and model 2, see text) are given as thick lines. The boxes and connected circles indicate the range of experimental data, as given by Robie and Hemingway (1984).

used infrared (IR) and Raman spectroscopic data in a calculation of the phase boundary between sillimanite and andalusite, and they estimated that the triple point occurs around 643–663 K and 3.0–3.2 kbar, excluding all effects due to lattice faults and Al-Si disorder. Salje (1986) measured heat capacities of samples of andalusite and sillimanite of different origins. He determined the influence of fibrolitization on the P,T dependence of the univariant reaction curve between andalusite and sillimanite. Using the previously published standard entropy of andalusite (Robie and Hemingway, 1984) and a standard entropy for sillimanite calculated from Raman and IR spectroscopic data, Salje (1986) determined the triple point in a system containing ideal sillimanite to be at 715 K and 3.2 kbar, whereas the measured triple point of bulky sillimanite was determined to be at 795 ± 15 K and 4.2 ± 0.2 kbar. The possibility of Al-Si disorder in sillimanite has been a controversial subject (Ribbe, 1982), but Holland and Carpenter (1984) concluded that "stoichiometric sillimanite is ordered at all geological temperatures." We therefore did not include any Al-Si disorder in our model.

Table 2. Comparison of the experimentally determined and the calculated phase diagram of the Al_2SiO_5 polymorphs

	Thermal expansion coefficients, α, and compressibilities, β			
	Andalusite		Sillimanite	Kyanite
α (10^5 K^{-1})	2.394		1.386	2.596
β (kbar^{-1})	0.67		0.65	0.70
	Measured and calculated values for the triple point			
790 ± 25 K	4.0 ± 0.5 kbar (Robie and Hemingway, 1984, exp)			
693 – 713 K	3.0 – 3.2 kbar (Salje and Werneke, 1982a, 1982b, calc)			
715 K	3.2 kbar (Salje, 1986, ideal sillimanite)			
800 K	4.2 kbar (this work, model 1)			
750 K	4.0 kbar (this work, model 2)			
	Slope of univariant reaction boundaries			
	Experimental		Model 1	Model 2
And-Sill	−19.5 bar/K	(790 < T < 850 K)		
	−13.5 bar/K	(T > 850 K)	−19.2 bar/K	−13.3 bar/K
And-Ky	11.8 bar/K		17.6 bar/K	17.0 bar/K
Sill-Ky	20.1 bar/K		26.3 bar/K	45 bar/K

Note: The thermal expansion coefficients, α, were calculated from the molar volume data at 298 and 873 K from Winter and Ghose (1979); the compressibilities, β, were taken from Brace et al. (1969); the slopes of the experimentally determined reaction boundaries are those given by Robie and Hemingway (1984).

We found that, in order to model the different structures of the polymorphs successfully, it is necessary to include a bond-bending term for all Al polyhedra. The calculated lattice parameters deviate only in one case by more than 2% (Table 3) from the experimentally determined data, and we note that the cell angles for triclinic kyanite are calculated to within 0.6°. The calculated atomic coordinates are compared with experimental data in Tables 4–6. The agreement is generally good. The major discrepancy is that the model underestimates the length of the anomalously short O(3)–O(3) distance. The calculated value of 2.06 Å is considerably less than the experimental value of 2.26 Å. This contact occurs within the five-coordinated Al polyhedron and points to inadequacies in the model at this point. Further investigation showed that the value for θ_0 used in the calculations is close to the optimum value, suggesting that improvements to the model will lie in finding a better value for the strength of the bond-bending force constant for this coordination. The calculated elastic constants of andalusite and sillimanite are compared in Table 3 to measured values (Vaughan and Weidner, 1978); no experimental values are available for kyanite. The agreement is reasonably good, taking into account the fact that only the off-diagonal elements of the elastic constant tensor deviate by more than 15% from measured values in andalusite. The only major discrepancy is for C_{33} in sillimanite; there are, however, no two independent experimental studies available. As we are confident in the predictive value of our calculations, we also give our calculated values for the diagonal elements of the elastic constant tensor for kyanite (Table 3).

The calculated vibrational frequencies can be compared with spectroscopic data. The experimentally determined frequency range for optic modes at the Γ point is 87–1113 cm^{-1} for andalusite and 70–1170 cm^{-1} for sillimanite (Salje and Werneke, 1982a, 1982b). The calculated frequencies range from 87 to 1012 cm^{-1} for anda-

Table 3. Comparison of experimental and calculated lattice parameters, molar volumes (V), and main-diagonal components of the elastic tensor (C_{ii}, units of Mbar) for the three Al_2SiO_5 polymorphs

	Andalusite		Sillimanite		Kyanite	
	exp	calc	exp	calc	exp	calc
a (Å)	7.7980	7.755	7.4883	7.271	7.1262	6.976
b (Å)	7.9031	7.808	7.6808	7.514	7.8520	7.829
c (Å)	5.5566	5.556	5.7774	5.862	5.5724	5.589
α (°)	90.0	90.0	90.0	90.0	89.99	90.55
β (°)	90.0	90.0	90.0	90.0	101.11	101.37
γ (°)	90.0	90.0	90.0	90.0	106.03	106.16
V (cm^3 mol^{-1})	51.58	50.67	50.049	48.23	44.22	43.16
	exp	calc	exp	calc	exp	calc
C_{11}	2.33	2.64	2.87	2.85	—	3.79
C_{22}	2.89	2.54	2.32	2.77	—	4.39
C_{33}	3.80	4.38	3.88	5.39	—	5.03
C_{44}	1.00	0.85	1.22	1.30	—	2.11
C_{55}	0.88	0.81	0.81	0.89	—	1.05
C_{66}	1.12	1.20	0.89	0.85	—	1.02

Note: Experimentally determined lattice parameters were taken from Winter and Ghose (1979). Measured elastic constants are from Vaughan and Weidner (1978).

TABLE 4. Observed and calculated fractional atomic coordinates of andalusite

	x_{obs}	y_{obs}	z_{obs}	x_{calc}	y_{calc}	z_{calc}
Al(1)	0.0	0.0	0.2419	0.0	0.0	0.2459
Al(2)	0.3705	0.1391	0.5	0.3680	0.1395	0.5
Si(1)	0.2460	0.2520	0.0	0.2356	0.2544	0.0
O(1)	0.4233	0.3629	0.5	0.4417	0.3555	0.5
O(2)	0.4246	0.3629	0.0	0.4209	0.3639	0.0
O(3)	0.1030	0.4003	0.0	0.0975	0.4104	0.0
O(4)	0.2305	0.1339	0.2394	0.2210	0.1438	0.2315

Note: Observed values were taken from Winter and Ghose (1979).

lusite and from 52 to 1053 cm^{-1} for sillimanite; in general, we have found that the calculations give frequencies that are slightly lower than experimental data, as in this case. Detailed comparisons of the Γ point frequencies with spectroscopic data and of the low-frequency dispersion curves with new inelastic neutron scattering data for andalusite are given in Winkler and Buehrer (1990). The overall comparison shows that the model gives a reasonable representation of the phonon frequencies for all wavevectors.

The HLDC results were used to calculate the thermodynamic properties of andalusite and sillimanite. A comparison of experimental data for the heat capacities, as published by Salje and Werneke (1982a, 1982b), is given in Figures 2 and 3. The agreement between calculation and experiment is very good if the sampling is performed over more than one point in the Brillouin zone; for the Al_2SiO_5 polymorphs, we used the Γ point and seven points on the faces of the Brillouin zone, (0 0 ½, 0 ½ ½, ½ ½ ½, etc.). Deviations from the expected behavior at $T < 50$ K are due to the coarse sampling of the Brillouin zone (see above).

We calculated the phase diagram of the system using two models. Model 1 was based on the molar volumes taken from Robie and Hemingway (1984), whereas model 2 was based on the molar volumes from our SLEC. The respective values are given in Table 3. In both models, the same thermal expansion coefficients for the polymorphs and the same compressibilities were employed. The former were calculated from the molar volumes of the polymorphs at 298 and 873 K as given by Winter and Ghose (1979), and the small temperature dependencies of the thermal expansion coefficients were neglected. The compressibilities were taken from Brace et al. (1969). The respective values are given in Table 2. Equilibrium points were taken to lie on the andalusite-sillimanite boundary at 1048 K and 1 bar and on the andalusite-kyanite boundary at 666 K and 2.4 kbar. The $\Delta S(T)$ was taken from our HLDC. The calculated phase diagrams are compared to the one given by Robie and Hemingway (1984) in Figure 1 and Table 2. The sillimanite-kyanite curve did not cross the triple point as determined by the kyanite-andalusite and andalusite-sillimanite reaction curves in either of the models when we used any of the equilibrium points given by Robie and Hemingway (1984). The triple points using the kyanite-sillimanite and andalusite-sillimanite reaction curves would be at approximately 890 K and 4 kbar in model 1 and at 890 K and 2 kbar in model 2. In general, model 1 shows a satisfactory agreement for all three univariant reaction boundaries, whereas model 2, although giving reasonable kyanite-andalusite and andalusite-sillimanite reaction curves, yields a kyanite-sillimanite reaction curve with far too steep a slope.

We conclude that the model used in the present study may be used in equilibrium thermodynamic studies, provided that additional experimental data for thermal expansions, compressibilities, and molar volumes are avail-

TABLE 5. Observed and calculated fractional atomic coordinates of kyanite

	x_{obs}	y_{obs}	z_{obs}	x_{calc}	y_{calc}	z_{calc}
Al(1)	0.3254	0.7040	0.4582	0.3348	0.7061	0.4607
Al(2)	0.2974	0.6989	0.9505	0.3033	0.7006	0.9518
Al(3)	0.0998	0.3862	0.6403	0.1004	0.3825	0.6367
Al(4)	0.1120	0.9175	0.1649	0.1174	0.9230	0.1689
Si(1)	0.2962	0.0649	0.7066	0.2947	0.0583	0.7091
Si(2)	0.2910	0.3317	0.1892	0.2871	0.3365	0.1828
O(1)	0.1095	0.1468	0.1288	0.0964	0.1482	0.1237
O(2)	0.1230	0.6856	0.1812	0.1234	0.6845	0.1825
O(3)	0.2747	0.4545	0.9547	0.2838	0.4584	0.9451
O(4)	0.2831	0.9354	0.9353	0.2961	0.9375	0.9491
O(5)	0.1219	0.6307	0.6389	0.1235	0.6325	0.6409
O(6)	0.2822	0.4453	0.4288	0.2911	0.4476	0.4346
O(7)	0.2915	0.9467	0.4659	0.3068	0.9495	0.4646
O(8)	0.5008	0.2749	0.2440	0.4924	0.2620	0.2376
O(9)	0.1084	0.1520	0.6669	0.0967	0.1435	0.6563
O(10)	0.5015	0.2312	0.7553	0.4937	0.2417	0.7585

Note: Observed values were taken from Winter and Ghose (1979).

TABLE 6. Observed and calculated fractional atomic coordinates of sillimanite

	x_{obs}	y_{obs}	z_{obs}	x_{calc}	y_{calc}	z_{calc}
Al(1)	0.0	0.0	0.0	0.0	0.0	0.0
Al(2)	0.1417	0.3449	0.25	0.1372	0.3441	0.25
Si	0.1533	0.3402	0.75	0.1530	0.3330	0.75
O(1)	0.3605	0.4094	0.75	0.3663	0.4012	0.75
O(2)	0.3569	0.4341	0.25	0.3574	0.4367	0.25
O(3)	0.4763	0.0015	0.75	0.4726	0.9998	0.75
O(4)	0.1252	0.2230	0.5145	0.1246	0.2176	0.5129

Note: Observed values were taken from Winter and Ghose (1979).

able. As discussed above, it should, in principle, be possible to determine these quantities from free energy minimization calculations (Parker and Price, 1989; Collins and Catlow, 1990). One difficulty in the present case is that we expect different energies for four-, five-, and six-coordinated Al because of covalent effects that the model does not attempt to handle—the model is really only designed to get the first and second differentials correct. We therefore cannot expect to be able to compare the energies of the three phases and have had to include experimental state points in our calculation of the phase boundaries. Price and Parker (1988) did not face this problem in their determination of the olivine-spinel phase diagram.

DIOPSIDE

Diopside, $CaMgSi_2O_6$, is a good example of a chain silicate ($C2/c$, $Z = 4$). SLEC, using models almost identical to those used in this study, have recently been discussed in some detail (Dove, 1989). The bond-bending potentials are essential in order to reproduce accurately the details of the structure, particularly with regard to the bond angles within the silicate chains, the Mg and Ca coordination, and the relative Si-O bond lengths for bridging and dangling bonds. Diopside has proven to be a demanding challenge for modelers (e.g., Post and Burnham, 1986).

We have performed additional calculations for diopside using our new value for the parameter K in Equation 10, and have also included diopside in this paper because

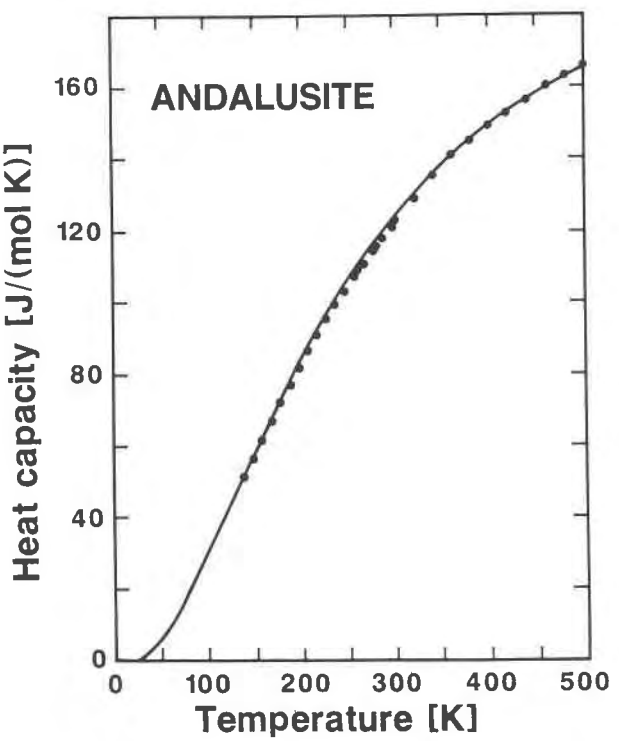

Fig. 2. Comparison of the experimentally determined heat capacity (C_p) of andalusite (points, Salje and Werneke, 1982a, 1982b) with calculated values (line). The deviation from the expected behavior at $T < 50$ K is due to the coarse sampling of the Brillouin zone (see text).

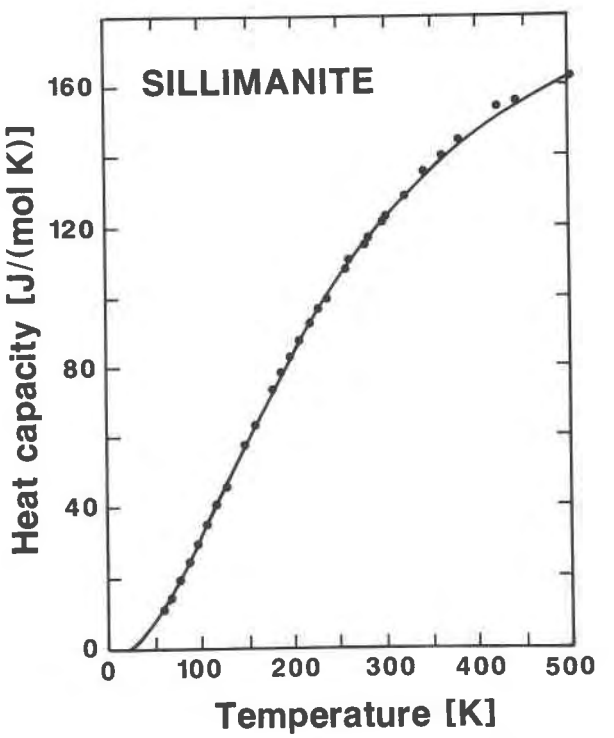

Fig. 3. Comparison of the experimentally determined heat capacity (C_p) of sillimanite (points, Salje and Werneke, 1982a, 1982b) with calculated values (line). The deviation from the expected behavior at $T < 50$ K is due to the coarse sampling of the Brillouin zone (see text).

TABLE 7. Comparison of observed and calculated structure and elastic constants of diopside

	Unit-cell parameters					
	obs	calc				
a (Å)	9.746	9.5197				
b (Å)	8.899	8.7096				
c (Å)	5.251	5.1496				
β (°)	105.63	104.47				
	Atomic fractional coordinates					
	x_{obs}	y_{obs}	z_{obs}	x_{calc}	y_{calc}	z_{calc}
Si	0.2862	0.0933	0.2293	0.2850	0.0970	0.2304
Mg	0.0	0.9082	0.25	0.0	0.9055	0.25
Ca	0.0	0.3015	0.25	0.0	0.3057	0.25
O(1)	0.1156	0.0873	0.1422	0.1105	0.0936	0.1442
O(2)	0.3611	0.2500	0.3180	0.3585	0.2571	0.3288
O(3)	0.3505	0.0176	0.9953	0.3615	0.0213	0.9950
	Elastic constants (Mbar)					
	obs	calc		obs		calc
C_{11}	2.23	2.68	C_{12}	0.77		1.20
C_{22}	1.71	1.99	C_{13}	0.81		1.06
C_{33}	2.35	2.72	C_{23}	0.57		0.85
C_{44}	0.74	0.65	C_{15}	0.17		0.20
C_{55}	0.67	0.80	C_{25}	0.07		0.04
C_{66}	0.66	0.98	C_{35}	0.43		0.62
			C_{46}	0.07		0.04

Note: Observed structural data were taken from Clark et al. (1969); elastic constant data are from Levien et al. (1979).

we wanted to include diopside, as a chain structure, in the data base for more detailed analysis. The results for the calculated equilibrium structure are given in Table 7, where they are compared with the results of the structure refinement of Clark et al. (1969). The differences from the results of previous calculations (Dove, 1989) are only slight, but nevertheless represent a modest improvement on the agreement with experimental data. We recall that the conclusion reached from the previous calculations (Dove, 1989) was that the chain structure, differences in the Si-O bond lengths, and the Mg and Ca coordinations can all be reproduced by the model; this conclusion holds with the modified core-shell interaction parameter.

CORDIERITE

Cordierite ($Mg_2Si_5Al_4O_{18}$) is of interest because it exists as either of two polymorphs, an ordered orthorhombic phase (*Cccm*, $Z = 4$) or a hexagonal phase with Al-Si site disorder (*P6/mcc*, $Z = 2$). We have modeled both phases.

Hexagonal cordierite contains two nonequivalent tetrahedral sites: site 1 [denoted T(1)] with ⅓ Al and ⅔ Si, and site 2 [denoted T(2)] with ⅔ Al and ⅓ Si (Dove et al., in preparation). Effective interactions were constructed using Equations 15–20 for both sites. The calculated equilibrium crystal structure for this model is compared with the experimental structure (Dove et al., in preparation; Armbruster, 1985) in Table 8. The agreement is satisfactory. It should be noted that the energy minimization was performed starting from an orthorhombic structure with only two types of tetrahedral sites. That the energy minimization yielded the hexagonal structure shows that the observed phase transition to the orthorhombic phase is triggered only by Al-Si ordering. This is consistent with kinetic observations but is different from the case of leucite (see below).

Coordinates and other data for the relaxed structure of the fully ordered orthorhombic form are compared with those of the experimental structure (Dove et al., in preparation; Gibbs, 1966; Cohen et al., 1977) in Table 9. There is again satisfactory agreement. But of greater significance than the comparison of the absolute structures is the calculation of the distortion of the structure of the ordered

TABLE 8. Crystal structure of hexagonal cordierite

	Unit-cell parameters					
	obs	calc				
a (Å)	9.7683	9.8548				
c (Å)	9.3408	9.1134				
	Atomic fractional coordinates					
	x_{obs}	y_{obs}	z_{obs}	x_{calc}	y_{calc}	z_{calc}
Mg	⅓	⅔	¼	⅓	⅔	¼
T(1)	½	½	¼	½	½	¼
T(2)	0.3724	0.2662	0	0.3693	0.2628	0
O(1)	0.4853	0.3492	0.1439	0.4846	0.3461	0.1479
O(2)	0.2304	0.3081	0	0.2315	0.3080	0

Note: Observed values are from Dove et al. (in preparation), which are consistent with Armbruster (1985). T denotes a tetrahedral site.

TABLE 9. Data for the crystal structure of orthorhombic cordierite

	Unit-cell parameters					
	obs	calc				
a (Å)	17.0448	17.1674				
b (Å)	9.7127	9.7517				
c (Å)	9.3318	9.0661				
e_s	0.00655	0.00813				
	Atomic fractional coordinates					
	x_{obs}	y_{obs}	z_{obs}	x_{calc}	y_{calc}	z_{calc}
Mg	0.3372	0.0	0.25	0.3367	0.0	0.25
Al(1)	0.25	0.25	0.2541	0.25	0.25	0.2537
Al(2)	0.0511	0.3080	0.0	0.0503	0.3031	0.0
Si(1)	0.0	0.5	0.25	0.0	0.5	0.25
Si(2)	0.1927	0.0789	0.0	0.1913	0.0766	0.0
Si(3)	0.1349	−0.2363	0.0	0.1319	−0.2355	0.0
O(1)	0.2461	−0.1029	0.3572	0.2466	−0.1001	0.3539
O(2)	0.0630	−0.4152	0.3494	0.0637	−0.4144	0.3483
O(3)	−0.1730	−0.3100	0.3585	−0.1700	−0.3110	0.3538
O(4)	0.0439	−0.2515	0.0	0.0405	−0.2351	0.0
O(5)	0.1216	0.1863	0.0	0.1218	0.1829	0.0
O(6)	0.1636	−0.0800	0.0	0.1713	−0.0844	0.0

Note: Observed data are from Dove et al. (in preparation), which are consistent with Gibbs (1966) and Cohen et al. (1977); e_s is the spontaneous strain defined by Equation 21.

phase from the hexagonal structure of the disordered form. This is quantified by the spontaneous strain, e_s, defined as

$$e_s = \frac{a - \sqrt{3}b}{a + \sqrt{3}b} \tag{21}$$

where a and b are the orthorhombic unit-cell parameters ($a = \sqrt{3}b$ in the hexagonal phase). The calculated and observed values of e_s are, respectively, 0.0081 and 0.0066 (Dove et al., in preparation). The size of this strain is slightly smaller than the differences between the calculated and observed cell lengths and thereby provides a subtle test of the predictive ability of these models. The agreement between the calculated and observed values of e_s is encouraging.

GEHLENITE

The crystal structure of gehlenite, $Ca_2Al_2SiO_7$, is tetragonal ($P\bar{4}2_1m$, $Z = 4$). The main feature of the structure is that it is composed of layers of five-membered rings of tetrahedra, with Ca in the large gaps between the layers. These features make gehlenite a useful system for testing transferable potential models. There are two distinct tetrahedral sites in the structure. The first site, T(1), is at the origin of the unit cell and has $\bar{4}$ symmetry. Crystal structure analysis has shown that this site contains Al (Kimata and Ii, 1982; Swainson et al., in preparation). The second site, T(2), is disordered, containing ½ Al and ½ Si. The effective potential for this site was again calculated from Equations 15–20. The results of the SLEC are given in Table 10, where they are compared with those of the observed structure (Swainson et al., in preparation; Kimata and Ii, 1982). The agreement is reasonable, and the model correctly reproduces the different T(2)-O bond lengths. The model also reproduces the Ca coordination satisfactorily.

LEUCITE

Leucite, $KAlSi_2O_6$, is a framework structure ($I4_1/a$, $Z = 8$), which is an ideal system for testing model potentials because the tetragonal structure is a slight distortion from a high-temperature cubic structure ($Im\bar{3}m$, $Z = 8$). A good model, therefore, should be able to reproduce this

TABLE 10. Crystal structure data for gehlenite

	Unit-cell parameters					
	obs	calc				
a (Å)	7.6850	7.5915				
c (Å)	5.0636	4.8964				
	Atomic fractional coordinates					
	x_{obs}	y_{obs}	z_{obs}	x_{calc}	y_{calc}	z_{calc}
Ca	0.3389	0.1611	0.5104	0.3407	0.1593	0.5172
T(1)	0.1434	0.3566	0.9540	0.1426	0.3574	0.9572
T(2)	0.0	0.0	0.0	0.0	0.0	0.0
O(1)	0.5	0.0	0.1765	0.5	0.0	0.1963
O(2)	0.1428	0.3572	0.2835	0.1406	0.3594	0.2997
O(3)	0.0876	0.1676	0.8077	0.0928	0.1649	0.7953

Note: Observed data are from Swainson et al. (in preparation), which are consistent with Kimata and Ii (1982). T(1) is occupied by Al and T(2) is occupied by $Al_{0.5}Si_{0.5}$, as described in the text.

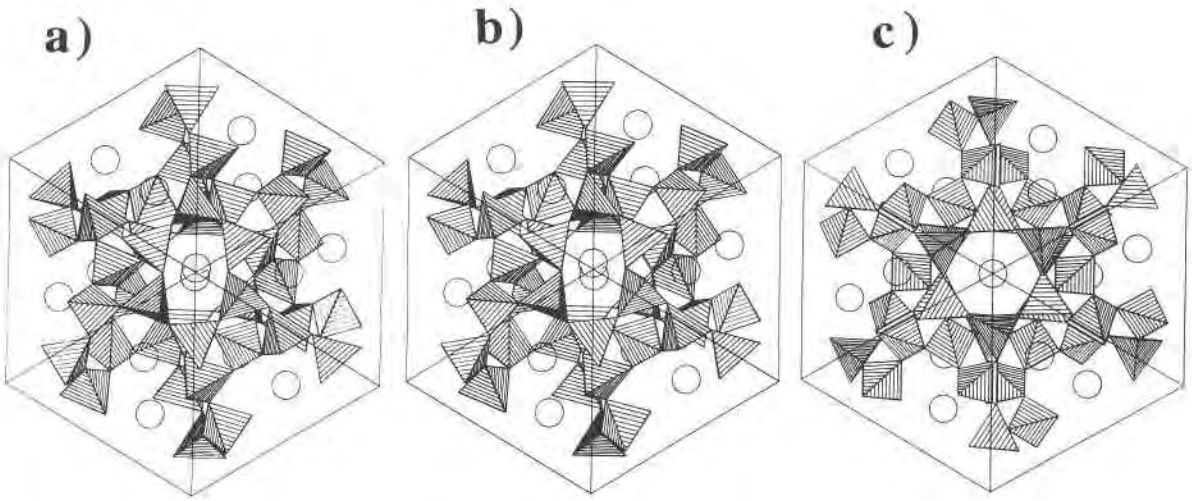

Fig. 4. Projection down [1$\bar{1}$1] of the structure of leucite: (**a**) observed tetragonal structure at room temperature, (**b**) calculated tetragonal structure, (**c**) observed cubic structure. The comparison of **a** and **b** shows that our model has reproduced the tetragonal distortion from **c**. Observed structure data are from Dove and Palmer (in preparation).

small distortion. In the cubic phase (which is stable above 940 K), there is only one symmetrically distinct tetrahedral site, so this phase must have no long-range Al-Si site order. There are no other sites (e.g., octahedral) in either phase for Al or Si atoms. The cubic-to-tetragonal phase transition occurs much faster than would be expected for a transition due to Al-Si ordering (Palmer et al., 1989; Palmer et al., 1990; Heaney and Veblen, 1990). Therefore, we would expect the tetragonal phase to remain disordered. This has been confirmed by diffraction experiments (Mazzi et al., 1976; Grogel et al., 1984; Dove and Palmer, in preparation), which are sensitive to long-range order, although there is evidence (albeit contradictory) for the existence of short-range order from nuclear magnetic resonance experiments (Brown et al., 1987; Murdoch et al., 1988; Phillips et al., 1989).

Effective interactions for the tetrahedral sites were constructed assuming complete Al-Si disorder [i.e., each site contains (Al + 2Si)/3] and using one mean bond length obtained from the three sites in the tetragonal structure. It should be noted that leucite is our only example that tests the K-O potential parameters.

The tetragonal structure could be relaxed easily, since it is the stable leucite structure. A straightforward energy minimization allowing for changes in the cell volume was not possible because the cubic structure is unstable with respect to the tetragonal distortion and the program THB_REL does not incorporate the use of constraints on the symmetry of the structure or on the shape of the unit cell. We therefore carried out a number of constant-volume energy minimizations of the cubic structure, using different unit-cell edge lengths. We then fitted the minimum energies to a fourth-order polynomial in the cubic unit-cell edge length. The strain-free unit-cell edge length was obtained from the minimum of this polynomial, and another structure relaxation was carried out using this value for the unit-cell edge length. The results of this energy minimization confirmed that the relaxed structure was actually free of all residual stresses.

The results of SLEC for both the tetragonal and cubic phases are given in Table 11, where they are compared with observed results (Dove and Palmer, in preparation; Mazzi et al., 1976; Grogel et al., 1984). The details are best discussed with reference to Figure 4, which shows the [1$\bar{1}$1] projection of the tetragonal phase as determined by experiment and as given by SLEC, together with the same projection of the cubic phase as determined by diffraction data. This projection highlights the loss of the three-fold axis on transformation from the cubic to the tetragonal form. The key features to note are the distortion of the six-membered ring of tetrahedra surrounding the [1$\bar{1}$1] axis and the off-centering of the K ions. Both of these features are reproduced remarkably well in our calculations.

The transition also involves a change in volume and a spontaneous strain (Palmer et al., 1989). Palmer et al. (1989) define the two strain parameters e_a and e_3:

$$e_a = \frac{a_0 - \tilde{a}_0}{\tilde{a}_0} \tag{22}$$

$$e_3 = \frac{c - \tilde{a}_0}{\tilde{a}_0} \tag{23}$$

where a and c are the tetragonal unit-cell lengths, a_0 is the actual cubic unit-cell length, and $\tilde{a}_0$ is given by

$$\tilde{a}_0 = \frac{c + 2a}{3}. \tag{24}$$

The $\tilde{a}_0$ would be equal to a_0 if the transition were purely ferroelastic, but experimentally it is found that these two quantities have very different values. Hence e_3 gives a measure of the pure ferroelastic strain, and e_a gives a

TABLE 11. Crystal structure and spontaneous strain parameters of leucite

Unit-cell parameters and spontaneous strain parameters						
	obs	calc				
a (Å)	13.0897	12.9884				
c (Å)	13.7530	13.8000				
a_0 (Å)*	14.38**	13.6444†				
$\hat{a}_0$ (Å)*	13.3108	13.2589				
e_3*	0.0332	0.0408				
e_a*	0.013	0.0291				
Fractional atomic coordinates for the tetragonal phase						
	x_{obs}	y_{obs}	z_{obs}	x_{calc}	y_{calc}	z_{calc}
K	0.3663	0.3654	0.1171	0.3659	0.3631	0.1073
T(1)‡	0.0582	0.3967	0.1654	0.0563	0.3971	0.1671
T(2)‡	0.1685	0.6124	0.1279	0.1668	0.6115	0.1269
T(3)‡	0.3933	0.6406	0.0863	0.3929	0.6407	0.0848
O(1)	0.1308	0.3136	0.1111	0.1327	0.3162	0.1097
O(2)	0.0927	0.5105	0.1310	0.0881	0.5135	0.1329
O(3)	0.1455	0.6790	0.2269	0.1459	0.6819	0.2257
O(4)	0.1342	0.6839	0.0358	0.1325	0.6857	0.0359
O(5)	0.2892	0.5773	0.1212	0.2894	0.5733	0.1183
O(6)	0.4841	0.6175	0.1665	0.4839	0.6161	0.1658
Mean T-O bond lengths (in Å) for the tetragonal phase§						
	obs	calc	cubic phase			
T(1)-O	1.642(17)	1.646(6)	1.622(2)			
T(2)-O	1.648(10)	1.654(15)	—			
T(3)-O	1.658(12)	1.663(4)	—			
Atomic coordinates for the cubic phase						
	x_{obs}	y_{obs}	z_{obs}	x_{calc}	y_{calc}	z_{calc}
K	0.375	0.375	0.125	0.375	0.375	0.125
T‡	0.0878	0.375	0.1622	0.0877	0.375	0.1623
O	0.1329	0.2806	0.1034	0.1354	0.2813	0.1035

Note: Observed data are from Palmer et al. (1989) and Dove and Palmer (in preparation). The observed structure data are consistent with Mazzi et al. (1976) and Grogel et al. (1984).

* Quantities defined in the text by Equations 22–24.

** Value obtained by extrapolation from high temperature data.

† Value obtained from energy minimization of cubic structure.

‡ T denotes disordered tetrahedral site containing $Al_{1/3}Si_{2/3}$.

§ Quantities in brackets give standard deviations over four bond lengths.

measure of the nonferroelastic strain. Most of the volume change associated with the phase transition is due to the nonferroelastic strain e_a.

The observed and calculated values for these strain quantities are given in Table 11. Although the calculated value of the ferroelastic strain e_3 agrees well with the experimental value, there is a difference of a factor of 2 between the calculated and observed values of the nonferroelastic strain e_a. This is principally due to the fact that the calculated cubic unit-cell edge length, a_o, differs from the experimentally determined value by more than the differences between any of the other calculated and observed lengths. That said, the discrepancy is as small as 1.2%, so we are really talking of small errors that are greatly magnified when subtracting two similar large numbers. It should be noted that the experimental value of a_o was obtained by extrapolation over a range of 650 K away from the actual experimental data, but the discrepancy between the calculated and observed values cannot be fully accounted for by postulating the existence of undetected errors in the extrapolation procedure. The discrepancies that we have pointed out should not detract from the fact that the model has given the essential qualitative details of the strain distortions, which means that the model correctly reproduces the couplings between the order parameters associated with the symmetry changes and the spontaneous strains.

We can therefore conclude that the basic model is able to reproduce the phase transition behavior in leucite, with the correct couplings between the framework distortions, K ion displacements, and volume and strain distortions.

One other feature of the tetragonal structure that is of interest is the range of tetrahedral bond lengths. In the tetragonal phase there are three nonequivalent tetrahedral sites, so in principle there could be some Al-Si ordering. An analysis of the experimental bond lengths has suggested that the degree of any ordering will be small, but it has been noted that the bond lengths for the different sites are not equal. Our model has used identical potentials for each of the sites (the assumption of complete disorder). The calculated structure gives unequal bond lengths similar to those calculated from the observed structure parameters (Table 11). We can therefore conclude that the experimental structures are consistent with the complete lack of any long-range Al-Si order. We can also conclude that the observed strain distortions are not caused by Al-Si ordering. This has been confirmed by a calculation for a hypothetical ordered structure, with Al on the T(2) site and Si on the other two tetrahedral sites. The strain distortions given by this structure were barely

different from the strain distortions given by our disordered model. A more detailed study elucidating the role of Al-Si ordering will be presented elsewhere (Dove et al., in preparation).

Zoisite

Zoisite, $Ca_2Al_3[O/OH/SiO_2/Si_2O_7]$, is an Fe-free orthorhombic (*Pnma*, $Z = 4$) end-member of the epidote group. The structure, as determined by Dollase (1968), contains SiO_4 and Si_2O_7 groups, as well as chains of edge-sharing Al octahedra running parallel to [010]. H bonds are located between these chains. The Ca atoms are situated in irregular polyhedra. If a cutoff value of 2.85 Å for bond lengths is used, both independent Ca atoms are seven coordinated (Dollase, 1968).

Not only is the complexity of this structure a challenge for modeling, but it is also a good test case for O-H potentials. Because of the relatively small numbers of H atoms, one can neglect direct non-Coulombic H-H interactions in a first approach. The modeling of OH groups is not straightforward. Different potentials have been proposed (Saul et al., 1985; Abbott et al., 1989a, 1989b; Collins and Catlow, 1990). The potentials suggested by Abbott et al. (1989a, 1989b) were derived from energy-minimum search calculations for brucite OH and mica OH in a number of structures (e.g., chlorite, clintonite, lizardite, tremolite). Abbott et al. (1989a, 1989b) suggested a value of $\rho = 2.5$ Å in Equation 12. They concluded that the O-H distances and orientations are modeled best with $B_{OH} = 30000$ kJ/mol for trioctahedral mica layers and tremolite, and $B_{OH} = 24250$ kJ/mol for brucite sheets in chlorite. O atoms were modeled as rigid ions with a formal charge of $-2e$, and H atoms were given the charge $+1e$. Collins and Catlow (1990) successfully modeled micas using a model similar to the one described in the present paper. They modeled the O-H interaction with the modified Morse function of Equation 14, the parameters for which are given in Table 1. The O in the O-H group was modeled as a rigid ion with a charge of $-1.426e$, whereas the H atom was assigned a charge of $+0.426e$. The O-H bond distance in the model was calculated to be about 6% larger than the experimentally determined one (Collins and Catlow, 1990). All other O atoms were modeled with a core and a shell. Neither model has been tested by HLDC, which we regard as the most stringent test of any O-H potential.

Dollase (1968) determined the O-H distance to be 1.2(2) Å and the length of the OH . . . H H bridge to be 2.76(2) Å. Linke (1970) confirmed by single-crystal polarized light IR spectroscopy that the O-H dipole is parallel to [001]. We tested the potential parameters of Abbott et al. (1989a, 1989b) and Collins and Catlow (1990) in our model of the zoisite structure. The potential parameters of Collins and Catlow (1990) did not work initially, because of the large attractive electrostatic forces on the H atoms from O atoms not belonging to the OH group. The inclusion of short-range repulsive interactions using the potential parameters of Abbott et al. (1989a, 1989b) led to a satisfactory relaxation of the structure. The calculated lattice parameters for both models are given in Table 12. As may be seen from Table 12, both models reproduced the orientation of the OH group with respect to the *c* axis very well. Both models gave an O-H bond distance that was too short, the modified Collins and Catlow model giving an even shorter bond than the Abbott et al. (1989a, 1989b) model. There are two different Ca polyhedra in zoisite structure. The O-Ca-O bond angles are modeled to better than 8° for polyhedra, whereas the bond lengths are all about 0.1 Å too short.

Table 12. Comparison of observed data and results of SLEC and HDLC for zoisite

	obs	Model 1	Model 2
a (Å)	16.193(2)	15.927	15.725
b (Å)	5.549(1)	5.534	5.608
c (Å)	10.036(2)	9.731	10.003
O-H (Å)	1.2(2)	1.126	0.983
<OH,[001]	0°	0.06°	0.02°
OH-O (Å)	2.75(2)	2.44	2.66
$\tilde{\nu}_{OH}$ (cm^{-1})	~3160	~2325	~4029
Other optic phonons	<1160 cm^{-1}	50–1069* cm^{-1}	50–1072 cm^{-1}

Note: Observed data were taken from Langer and Lattard (1980); model 1 uses the parameters of Abbott et al. (1989a, 1989b), and model 2 uses those of Collins and Catlow (1990) as described in the text.

* Excluding the modes related to the bending vibration of the H bond at ~1420 cm^{-1}.

HLDC were performed to elucidate the reliability of the OH potential further. We calculated the phonons at the Γ point. IR studies in the frequency range above 400 cm^{-1} were performed by several authors, e.g., Linke (1970), Langer and Raith (1974), Langer and Lattard (1980), and Winkler et al. (1989). The IR spectrum of zoisite in the region above 400 cm^{-1} may be subdivided into three regions: the OH stretching vibrations occur at around 3160 cm^{-1}, there is a distinct band at about 2160 cm^{-1}, and the normal lattice modes have wavenumbers <1160 cm^{-1}. The normal lattice modes below approximately 1160 cm^{-1} are correctly calculated using both models; the calculated frequency range is 50–1070 cm^{-1}. Langer and Lattard (1980) assigned the 2160 cm^{-1} band to an unusually strong, second H bridge. On deuteration this band shifts to lower frequencies (Langer and Lattard, 1980) and shifts to higher frequencies with increasing pressure (Winkler et al., 1989). Because of these shifts and the unlikelihood of the existence of such a strong H bridge in silicates [the stretching frequency is expected to shift from approximately 3700 cm^{-1} to 2160 cm^{-1} when the OH-O distance is approximately 2.5 Å (Nakamoto et al., 1955), Winkler et al., (1989) concluded that the previous assignment of Langer and Lattard (1980) was incorrect and suggested that, instead, the band was caused by a mode-mode coupling of the bending vibration of the H bond and a lattice mode. In general, the OH stretching frequency is a function of the OH-O distance and the O-H distance (Nakamoto et al., 1955; Novak, 1974). Both models gave O-H distances that were too short, and this

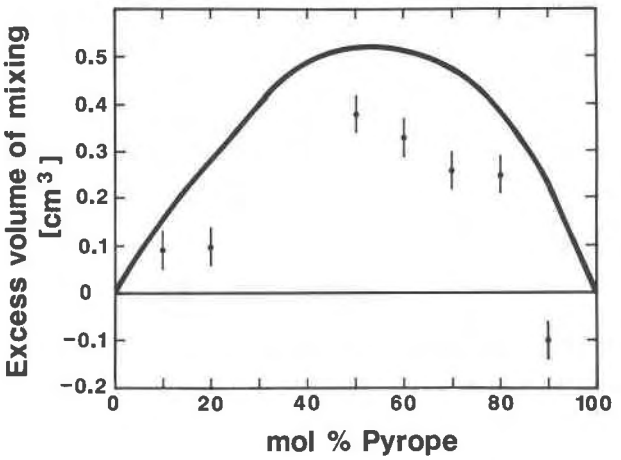

Fig. 5. Comparison of experimentally determined excess volume of pyrope-grossular garnets (points, Haselton and Newton, 1980) and calculated values (line). Note that there is no consensus on the best value for the lattice parameter of pyrope (see text).

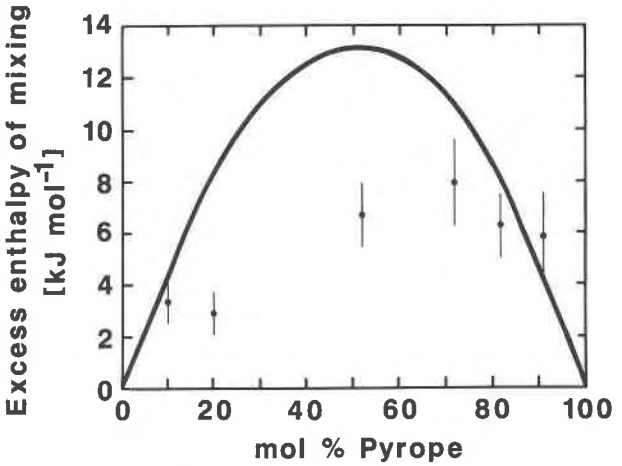

Fig. 6. Comparison of experimentally determined excess enthalpy of pyrope-grossular garnets (points, Haselton and Newton, 1980) and calculated values (line).

would increase the stretching frequency. On the other hand, both models also gave short OH-O distances, which would decrease the stretching frequency. The HLDC that we carried out using the model of Collins and Catlow (1990) did not give any modes with frequencies between 1073 cm^{-1} and the high OH stretching mode frequencies at 4032 cm^{-1}. The model with the potential parameters of Abbott et al. (1989a, 1989b) gave high-frequency modes at 1420 cm^{-1} and 2325 cm^{-1}. An analysis of the respective eigenvectors showed that the modes around 1420 cm^{-1} are caused by the bending vibration of the OH-O H bridge, whereas the modes around 2325 cm^{-1} were due to the OH stretching motion. As we are convinced that our HLDC are sufficiently reliable, we conclude that the experimentally determined vibration at approximately 2160 cm^{-1} is due to anharmonic effects. This supports the suggestion of Winkler et al. (1989) that this band is due to a coupling process.

Garnets

Aluminosilicate garnets have the general formula $A_3Al_2Si_3O_{12}$. They are cubic (*Ia3d*) with $Z = 8$ formula units per unit cell. We modeled grossular (gr) with A = Ca and pyrope (py) with A = Mg. To demonstrate that the potentials used are realistic enough to model small effects, like the excess volume of mixing and the excess enthalpy of mixing, we carried out calculations for solid solutions between the end-members. These are denoted by either py$X$gr$(10 - X)$ or gr$X$py $(10 - X)$. The mol% of the respective component divided by 10 is given as X. The end-member which is given first indicates the structure which was used at the beginning of the relaxation. The effective A-O potentials were constructed from Equations 19 and 20.

In general, excess properties deviate by less than 1% from the value which the respective property would have if ideal mixing took place. This ideal behavior can be obtained by linear interpolation between the end-members. Although the values of the excess properties are small, they are important for the P,T dependence of the thermodynamic functions. For this reason the mixing behavior of a large number of silicates and nonsilicates have been studied (e.g., Newton et al., 1977; Newton and Wood, 1980; Haselton and Newton, 1980). Haselton and Newton (1980) published a summary of the excess properties of py-gr solid solutions. Their results for the excess volume and excess enthalphy of mixing are given in Figures 5 and 6, respectively. We note that there seems to be no consensus as to the best value for the lattice constant of dry synthetic pyrope. Geiger et al. (in preparation) compared several observed cell parameters. For similar synthesis conditions (30–40 kbar, 1673–1723 K), the measured values ranged from 11.4540(5) to 11.459(1). If the value of 11.454 is taken, there is no region of negative excess volume.

The structures of the end-member garnets were modeled satisfactorily (Table 13). The calculated elastic constants are too large by approximately 20%. The excess volumes and enthalpies are given in Table 14 and Figures 5 and 6. We have assumed that the excess enthalpies are primarily due to excess lattice potential energy. The excess properties are calculated to within the correct order of magnitude. The experimentally determined excess volume deviates by only approximately 0.3% from the ideal behavior (Haselton and Newton, 1980) at py5gr5 composition. Our calculated value of 0.5% is therefore judged as satisfactory. Furthermore, Haselton and Newton (1980) point out that the excess volume is asymmetric. The magnitude of this asymmetry cannot be determined until more accurate data on the lattice parameters for this solid solution series, especially for the pyrope-rich members, become available. The model gives a slight asymmetry of the excess volume. The agreement between the calculated and observed values of the excess enthalpy is not as good

TABLE 13. Crystal structures and elastic constants (units of Mbar) of pyrope and grossular

	Pyrope		Grossular	
	obs	calc	obs	calc
a (Å)	11.454	11.302	11.846	11.565
x	0.0328	0.0311	0.0380	0.0356
y	0.0502	0.0549	0.0450	0.0515
z	0.6534	0.6526	0.6518	0.6506
C_{11}	2.87	3.39	3.22	3.97
C_{12}	1.05	1.32	0.91	0.98
C_{44}	0.92	1.15	1.05	0.94

Note: x, y, z are the fractional coordinates for the O atom; all other coordinates are defined for special positions of the space group. Observed data for the crystal structures were taken from Hazen and Finger (1978); elastic constants for pyrope are from Isaak and Graham (1976), and elastic constants for grossular are from Bass (1989).

as for the excess volume, although it should be noted that the size of the effect is as small as 0.02% of the calculated lattice energy.

Table 15 shows a comparison of some of the calculated $\mathbf{k} = 0$ optic mode frequencies for pyrope with corresponding experimental values determined by IR spectroscopy. The agreement is reasonably good. We have also calculated the specific heat and the entropy for pyrope. The density of states was calculated by using the mean point of the Brillouin zone of an I-centered cubic lattice at (⅙, ⅙, ½) (Baldereschi, 1973). The calculated values are compared with the data published by Haselton and Westrum (1980) in Table 16. The agreement with the experimental data is not as good as for other systems. We attribute this to the neglect of Mg anharmonicity or site disorder in the model, which will cause the entropy to be underestimated.

General analysis

The previous sections have shown that the basic potential model used in this paper is able to reproduce a wide range of aluminosilicate structures. A general quantitative assessment of the accuracy of the model is therefore possible. We need to define two standard deviations for this:

$$\sigma_D = \left[\frac{1}{N}\sum_{j=1}^{N}(P_j^{obs} - P_j^{calc})^2\right]^{1/2} \quad (25)$$

$$\sigma_{WD} = \left[\frac{1}{N}\sum_{j=1}^{N}\left(\frac{P_j^{obs} - P_j^{calc}}{P_j^{obs}}\right)^2\right]^{1/2} \quad (26)$$

where P^{obs} and P^{calc} are observed and calculated quantities (such as cell edges, bond lengths), respectively. N is the number of quantities used in the calculation of these standard deviations. The weighted deviation, σ_{WD}, gives a measure of the agreement as a proportion and will be used for quantities such as the unit-cell edges, which have a wide range of values. On the other hand, the quantity, σ_D, gives a measure of the absolute agreement and is useful for quantities such as bond lengths, which do not change much from one structure to another. It is instructive to compare calculated values of σ_D with the regular standard deviation for the experimental data, σ, given as

TABLE 14. Calculated mixing properites of pyrope-grossular solid solutions

	Molar volume (cm³/mol)	Excess volume (cm³/mol)	Lattice energy (eV/mol)	Excess energy (eV/mol)
pyrope	108.68	—	338.03	—
py9gr1	109.68	0.22	337.80	0.03
py7gr3	111.48	0.47	337.36	0.07
py6gr4	112.30	0.52	337.16	0.07
py5gr5	113.08	0.53	336.95	0.08
gr5py3	114.51	0.40	336.95	0.08
gr9py1	115.82	0.17	336.56	0.07
grossular	116.43	—	336.20	—

$$\sigma = \left[\frac{1}{(N-1)}\sum_{j=1}^{N}(P_j^{obs} - \bar{P})^2\right]^{1/2} \quad (27)$$

where $\bar{P}$ is the mean of the observations. We expect that σ_D will be less than σ if the model has given satisfactory results.

It should be noted that, in the analysis presented below, we have included the results from both models of zoisite. We have excluded the results for the cubic phase of leucite, since the experimental data are necessarily for high temperatures.

Unit-cell edge length

Averaging over all the cell edge lengths, we obtain

mean observed cell edge length = 9.3313 Å
mean calculated cell edge length = 9.2211 Å
$\sigma_{WD} = 0.0184$
$N = 36$.

The model, in general, reproduces the cell edge lengths to within 2%, which gives on average a slight underestimate of 1%.

Bond lengths

Averaging over all the Si-O bond lengths, we obtain

mean observed bond length = 1.628 Å (σ = 0.029 Å)
mean calculated bond length = 1.641 Å (σ = 0.041 Å)

TABLE 15. Calculated and observed T_{1u} $\mathbf{k} = 0$ optic phonon frequencies in pyrope

Obs (cm⁻¹)	Calc (cm⁻¹)
339	331
386	387
420	420
463	450
482	480
539	508
877	836
907	868
967	969

Note: Observed data were taken from Geiger et al. (1989).

Table 16. Heat capacities, C_P in (J mol^{-1} K^{-1}), and third law entropies, $S^\circ_T - S^\circ_0$ in (J mol^{-1} K^{-1}), of pyrope grossular garnets

	obs	calc
C_P, 150 K	171.5	157.75
C_P, 298 K	325.3	323.04
$S^\circ_T - S^\circ_0$, 150 K	95.56	74.45
$S^\circ_T - S^\circ_0$, 298 K	266.3	237.32

Note: Observed data were taken from Haselton and Westrum (1980); the C_V to C_P conversion factors were taken from Holland and Powell (1989).

$$\sigma_D = 0.021 \text{ Å}$$
$$\sigma_{WD} = 0.013$$
$$N = 30.$$

The model gives, in general, a slight overestimate, but nevertheless the bond lengths are reproduced to within 1%.

For Al-O bond lengths we need to consider both tetrahedral and octahedral bond lengths. From the averaging we obtain

mean observed tetrahedral bond length = 1.740 Å
(σ = 0.033 Å)
mean calculated tetrahedral bond length = 1.740 Å
(σ = 0.041 Å)
$\sigma_D = 0.017$ Å
$\sigma_{WD} = 0.010$
$N = 9$
mean observed octahedral bond length = 1.907 Å
(σ = 0.073 Å)
mean calculated octahedral bond length = 1.896 Å
(σ = 0.073 Å)
$\sigma_D = 0.037$ Å
$\sigma_{WD} = 0.019$
$N = 54.$

The agreement is comparable with the agreement for the Si-O bond lengths. It may seem remarkable that the use of a single Al-O interaction for both types of coordination polyhedra can give similar accuracy for both types of bond lengths.

The statistical analysis of all bond lengths shows that the model can give individual bond lengths to an accuracy of better than 2%. The mean calculated bond lengths are within 1% of the observed mean values. There is a distribution of actual bond length values in the different crystals, and our model reproduces this distribution.

Bond angles

We now perform a similar analysis for the tetrahedral and octahedral bond angles, including Si-O, Al-O and disordered bonds in the data set

mean observed tetrahedral angle = 109.49°
mean calculated tetrahedral angle = 109.44°
$\sigma_D = 1.38°$
mean absolute difference = 2.18°
$N = 72$
mean observed octahedral angle = 89.96°
mean calculated octahedral angle = 89.89°
$\sigma_D = 1.23°$
mean absolute difference = 1.85°
$N = 54.$

This analysis, and the previous bond length analysis, enables us to conclude that the size and shape of the Al-Si tetrahedra and octahedra can be accurately reproduced by the model for the whole range of different aluminosilicate structures studied. We are confident that other structures can be modeled with similar accuracy.

Cation coordination

The potentials we have used for Mg-O, Ca-O, and K-O interactions have been obtained independently of the Al-O and Si-O potentials described above. The averages over all the systems give

mean observed Mg-O distance = 2.136 Å (σ = 0.088 Å)
mean calculated Mg-O distance = 2.096 Å (σ = 0.078 Å)
$\sigma_D = 0.047$ Å
$\sigma_{WD} = 0.022$
$N = 8$
mean observed Ca-O distance = 2.575 Å (σ = 0.229 Å)
mean calculated Ca-O distance = 2.495 Å (σ = 0.246 Å)
$\sigma_D = 0.112$ Å
$\sigma_{WD} = 0.042$
$N = 35$
mean observed K-O distance = 3.028 Å (σ = 0.072 Å)
mean calculated K-O distance = 2.956 Å (σ = 0.065 Å)
$\sigma_D = 0.090$ Å
$\sigma_{WD} = 0.030$
$N = 6.$

We conclude from these figures that the model is also capable of reproducing the general cation-O bond lengths to within 4% in all cases, and the average bond lengths are in even better agreement.

Bond orientations

The structure is characterized by the size and shape of the coordination polyhedra, which we have shown are accurately reproduced by the model, and also by the orientations of the polyhedra. These orientations can be analyzed by considering the orientations of the individual bond vectors. We have calculated the root-mean-square angle between the observed and calculated bond vectors for the structures we have modeled:

tetrahedral (Si,Al)-O rms angle = 2.49°
octahedral Al-O rms angle = 2.24°
Mg-O rms angle = 1.88°
Ca-O rms angle = 2.51°
K-O rms angle = 2.13°.

The rms angle, in all cases, was found to be larger than the mean of the angle moduli. It is clear from this analysis that both the shapes and the orientations of the polyhedra are correctly given to within 2–3° on average. In the full analysis, the maximum difference was 6°.

There is an interesting interplay between short-range and long-range interactions in aluminosilicate structures. For any aluminosilicate structure, there will be a group of normal mode type distortions in which the basic rigid units (tetrahedra or octahedra) remain undistorted and only the connecting frameworks is distorted. These are called rigid-unit modes, and they form a small subset of the full set of allowed vibrational normal modes. The number of rigid-unit modes will depend on the structure, and the existence of any rigid-unit modes will also depend on the wavevector. This idea was first pointed out in connection with the phase transitions in quartz (Grimm and Dorner, 1975; Berge et al., 1986), and a general method for the evaluation of the set of rigid-unit modes in any crystal structure has been described by Giddy et al. (in preparation). From the point of view of structure modeling, the existence of rigid-unit modes presents an additional challenge since it is then possible to get the short-range aspects of the structure exactly correct (for example, the Si-O bond lengths) without consequently getting the framework structure correct to the same accuracy. The latter aspect is determined by the longer-range forces, namely the electrostatic interactions and the O . . . O dispersive interaction.

Summary

We have reported lattice energy minimization studies for a wide variety of aluminosilicate minerals, and we have augmented some of these with harmonic lattice dynamics calculations. Our primary aim has been to test one specific model, and we have been able to conclude that the basic model works rather well. We have made some minor modifications that we believe have improved the performance of the model. We have also introduced a method that can handle site occupancy disorder (either due to order-disorder phase transitions or solid solution formation), and we have shown that this method works well as far as the structures and energetics are concerned.

Our criteria for testing the potential model have gone beyond the reproduction of structures only; we are more interested in using the potentials in the study of more subtle effects, such as the properties associated with phase transitions. We have therefore used the model to predict a phase diagram (Al_2SiO_5) and to calculate the following: the coupling between an order-disorder phase transition and spontaneous strain distortions (cordierite), the similar couplings between a displacive phase transition and spontaneous strain distortions (leucite), departures from ideal solid solution behavior (pyrope-grossular solid solution), and thermodynamic quantities. We have found that the model always gives the correct qualitative behavior, and in many cases, we have found that the quantitative agreement between calculation and experiment is far better than one might have expected for such a simple model. The reader should note that these tests are pushing the model to limits beyond those for which it was designed. Although the discrepancies between calculated and observed properties point to inadequacies of the model, the essential result is that the model is nearly able to account correctly for such subtle effects.

If we combine our results with the results from the applications of this basic model to Mg_2SiO_4 (Price and Parker, 1988), SiO_2 (Sanders et al., 1984), and zeolites (Jackson and Catlow, 1988), we can conclude that the basic model described in this paper is a genuine transferable model that can be applied to a wide range of structure topologies (ortho-, chain-, layer-, and framework-aluminosilicates). It can model both structural and lattice dynamics aspects reasonably well. We have also tested the model on a number of other systems that have not been reported here (due to space limitations) and have found results that support our conclusion of the accuracy and transferability of the model.

However, we believe that the model can, and should, be improved, particularly with regard to the Al-O potentials. Although such an enterprise may seem daunting, the way ahead is clear. The potential parameters of the basic model can be refined by fitting calculated structures, elastic and dielectric constants, and vibrational frequencies to available observed data for a wide range of systems. This point was discussed by Dove (1989). Our own preliminary investigations of the model for andalusite have shown that minor modification of the value of the O-Al-O bond-bending force constant for the five-coordinated Al does lead to significant improvements in the resultant calculated structure. However, it is our opinion, supported by the experience of similar enterprises for modeling organic materials (Dove, 1989), that focusing on only a single system invariably leads to a potential model that is no more transferable than the starting point; instead, a wide number of structures is required for the development of a transferable model.

In the meantime, we believe that reliable results can still be obtained from studies using the model as it stands. One of the features we wish to highlight is the success of the potentials for Mg-O, Ca-O, and K-O interactions obtained from MEG calculations (Post and Burnham, 1986). We have also shown, in unreported work, that some of the other potentials given by Post and Burnham are equally useful. Additional potentials obtained by this method (e.g., for Rb-O and Cs-O interactions) would be extremely helpful.

We hope also that we have been able to demonstrate the predictive benefits of the model. This point has been exemplified by our discovery that the mechanism of the ferrodistortive phase transition in leucite is virtually independent of any Al-Si ordering. Our successful calculations of phase diagrams and excess properties of solid solutions also point to future applications of the model. It is our hope that the general analysis we have performed will now enable the model to be used with some confidence, given the knowledge of the limits of its reliability.

Acknowledgments

We thank Jennifer-Anne Dove for her encouragement. We are grateful to the authors of Abbott et al. (1989a, 1989b) and Collins and Catlow (1990) for sending us preprint copies of their papers. B.W. gratefully acknowledges a grant from the German Academic Exchange Service (DAAD). We are also grateful to Pat Hancock for her help in the preparation of this document. This is Earth Science Contribution ES 1765.

References cited

Abbott, R.N., Jr., Post, J.E., and Burnham, C.W. (1989a) Treatment of the hydroxyl in structure-energy calculations. American Mineralogist, 74, 141–150.

Abbott, R.N., Jr., Burnham, C.W., and Post, J.E. (1989b) Hydrogen in humite-group minerals: Structure-energy calculations. American Mineralogist, 74, 1300–1306.

Armbruster, T. (1985) Crystal structure, Si,Al-ordering, and twinning in "pseudo-hexagonal" Mg-cordierite. Neues Jahrbuch fuer Mineralogie Monatshefte, M6, 255–267.

Baldereschi, A. (1973) Mean value point in the Brillouin Zone. Physics Review B7, 12, 5212–5215.

Bass, J.D. (1989) Elasticity of grossular and spessartite garnets by Brillouin Spectroscopy. Journal of Geophysical Research, 94, B6, 7621–7628.

Berge, B., Baccheimer, J.P., Dolino, G., and Vallade, M. (1986) Inelastic neutron scattering study of quartz near the incommensurate phase transition. Ferrolectrics, 66, 73–84.

Born, M., and Huang, K. (1954) Dynamical theory of crystal lattices. Oxford University Press, Oxford, United Kingdom.

Brace, W.F., Scholtz, C.H., and La Mori, P.N. (1969) Isothermal compressibility of kyanite, andalusite and sillimanite from synthetic aggregates. Journal of Geophysical Research, 74, 2089–2098.

Brown, I.W.M., Cardile, C.M., Mackenzie, K.J.D., Ryan, M.J., and Meinhold, R.H. (1987) Natural and synthetic leucites studied by solid state 29-Si NMR and 57-Fe Mossbauer spectroscopy. Physics and Chemistry of Minerals, 15, 78–83.

Catlow, C.R.A. (1988) Computer modelling of silicates. In E.K.H. Salje, Ed., Physical properties and thermodynamic behaviour of minerals, NATO ASI Series C, vol. 225, p. 619–638, Reidel, Boston.

Catlow, C.R.A., Mackrodt, J.R., and Stewart, R.F. (1982) Defect energies in aluminium oxide and rutile titanium oxide. Physical Review B, 25, 1006–1026.

Clark, J.R., Appleman, D.E., and Papike, J.J. (1969) Crystal-chemical characterization of clinopyroxenes based on eight new structure refinements. Mineralogical Society of America Special Paper, 2, 31–50.

Cohen, J.P., Ross, F.K., and Gibbs, G.V. (1977) An X-ray and neutron diffraction study of hydrous low cordierite. American Mineralogist, 62, 67–78.

Collins, D.R., and Catlow, C.R.A. (1990) Interactive potentials for micas. Molecular Simulation, 4, 341–346.

Deer, W.A., Howie, R.A., and Zussman, J. (1966) An introduction to rock forming minerals. Longman, London.

Dollase, W.A. (1968) Refinement and comparison of the structures of zoisite and clinozoisite. American Mineralogist, 53, 1882–1898.

Dove, M.T. (1989) On the computer modeling of diopside: Toward a transferable potential for silicate minerals. American Mineralogist, 74, 774–779.

Geiger, C.A., Winkler, B., and Langer, K. (1989) Infrared spectra of synthetic almandine-grossular and aldamine-pyrope garnet solid solutions: Evidence for equivalent site behaviour. Mineralogical Magazine, 53, 231–237.

Gibbs, G.V. (1966) The polymorphism of cordierite I: The crystal structure of low cordierite. American Mineralogist, 51, 1068–1087.

Grimm, H., and Dorner, B. (1975) On the mechanism of the α-β phase transformation of quartz. Journal of Physics and Chemistry of Solids, 36, 407–413.

Grogel, T., Boysen, H., and Frey, F. (1984) Neutron powder investigation of $I4_1/a$-Ia3d in leucite. Collected abstracts of 13th international conference of crystallography, C256–257.

Haselton, H.T., and Newton, R.C. (1980) Thermodynamics of pyrope-grossular garnets and their stabilities at high temperatures and high pressures. Journal of Geophysical Research, 85, B12, 6973–6982.

Haselton, H.T., and Westrum, E.F. (1980) Low-temperature heat capacities of synthetic pyrope, grossular, and $pyrope_{60}grossular_{40}$. Geochimica et Cosmochimica Acta, 44, 701–709.

Hazen, R.M., and Finger, L.W. (1978) Crystal structures and compressibilities of pyrope and grossular to 60 kbar. American Mineralogist, 63, 297–303.

Heaney, P.J., and Veblen, D.R. (1990) A high-temperature study of the low-high leucite phase transition using the transmission electron microscope. American Mineralogist, 75, 477–489.

Holland, T.J.B., and Carpenter, M.A. (1984) Order-disorder in sillimanite. In C.M.B. Henderson, Ed., Progress in experimental petrology. The Natural Environmental Research Counsel Publications Series D, no. 25, p. 183–185.

Holland, T.J.B., and Powell, R. (1989) An enlarged and updated internally consistent thermodynamic dataset with uncertainties and correlations: The system K_2O-Na_2O-MgO-MnO-FeO-Fe_2O_3-Al_2O_3-TiO_2-SiO_2-C-H_2-O_2. Journal of Metamorphic Geology, in press.

Isaak, D.G., and Graham, E.K. (1976) The elastic properties of an almandine-spessartine garnet and elasticity in the garnet solid solution series. Journal of Geophysical Research, 81, 2483–2489.

Jackson, R.A., and Catlow, C.R.A. (1988) Computer simulation studies of zeolite structures. Molecular Simulation, 1, 207–224.

Kimata, M., and Ii, N. (1982) The structural properties of synthetic gehlenite $Ca_2Al_2SiO_7$. Neues Jahrbuch fuer Mineralogie Abhandlungen, 144, 254–267.

Langer, K., and Lattard, D. (1980) Identification of a low energy OH-valence vibration in zoisite. American Mineralogist, 65, 779–783.

Langer, K., and Raith, M. (1974) Infrared spectra of Al-Fe(III)-epidotes and zoisites, $Ca_2(Al_{1-p}Fe_p)Al_2O(OH)[Si_2O_7][SiO_4]$. American Mineralogist, 59, 1249–1258.

Lasaga, A.C., and Gibbs, G.V. (1987) Applications of quantum mechanical potential surfaces to mineral physics calculations. Physics and Chemistry of Minerals, 14, 107–117.

Levien, L., Weidner, D.J., and Prewitt, C.T. (1979) Elasticity of diopside. Physics and Chemistry of Minerals, 4, 105–133.

Linke, W. (1970) Messung des Ultrarot—Pleochroismus der OH Streckfrequenz in Zoisit. Tschermak's mineralogische und petrographische Mitteilunge, 14, 61–63.

Mazzi, F., Galli, E., and Gottardi, G. (1976) The crystal structure of tetragonal leucite. American Mineralogist, 61, 108–115.

Murdoch, J.B., Stebbins, J.F., Carmichael, I.S.E., and Pines, A. (1988) A silicon-29 nuclear magnetic resonance study of silicon-aluminum ordering in leucite and analcite. Physics and Chemistry of Minerals, 15, 370–382.

Nakamoto, K., Margoshes, M., and Rundle, R.E. (1955) Stretching frequencies as a function of distances in hydrogen bonds. Journal of the American Chemical Society, 77, 6480–6486.

Newton, R.C., Charlu, T.V., and Kleppa, O.J. (1977) Thermochemistry of high pressure garnets and clinopyroxenes in the system CaO-MgO-Al_2O_3-SiO_2. Geochimica et Cosmochimica Acta, 41, 369–377.

Newton, R.C., and Wood, B.J. (1980) Volume behavior of silicate solid solutions. American Mineralogist, 65, 733–745.

Novak, A. (1974) Hydrogen bonding in solids. Correlation of spectroscopic and crystallographic data. Structure and Bonding, 18, 177–216.

Palmer, D.C., Salje, E.K.H., and Schmahl, W.W. (1989) Phase transitions in leucite: X-ray diffraction studies. Physics and Chemistry of Minerals 16, 714–719.

Palmer, D.C., Bismayer, U., and Salje, E.K.H. (1990) Phase transition in leucite: Order parameter behaviour and the Landau potential deduced from Raman spectroscopy and birefringence studies. Physics and Chemistry of Minerals, 17, 259–265.

Parker, S.C., and Price, G.D. (1989) Computer modelling of phase transitions in minerals. Advances in Solid State Chemistry, 1, 295.

Phillips, B.L., Kirkpatrick, R.J., and Putnis, A. (1989) Si,Al ordering in leucite by high-resolution 27-Al MAS NMR spectroscopy. Physics and Chemistry of Minerals, 16, 591–598.

Post, J.E., and Burnham, C.W. (1986) Ionic modeling of mineral struc-

tures and energies in the electron gas approximation: TiO_2 polymorphs, quartz, forsterite, diopside. American Mineralogist, 71, 142–150.

Price, G.D., and Parker, S.C. (1988) The computer simulation of the lattice dynamics of silicates. In E.K.H. Salje, Ed., Physical properties and thermodynamic behaviour of minerals, NATO ASI Series C, vol. 225, p. 591–618. Reidel, Boston.

Ribbe, P.H. (1982) Kyanite, andalusite and other aluminum silicates. In Mineralogical Society of America, Reviews in Mineralogy, 5, 189–214.

Robie, R.A., and Hemingway, B.S. (1984) Entropies of kyanite, andalusite and sillimanite: Additional constraints on the pressure and temperature of the Al_2SiO_5 triple point. American Mineralogist, 69, 298–306.

Salje, E. (1986) Heat capacities and entropies of andalusite and sillimanite: The influence of fibrolitization on the phase-diagram of the Al_2SiO_5 polymorphs. American Mineralogist, 71, 1366–1371.

Salje, E., and Werneke, C. (1982a) The phase equilibrium between sillimanite and andalusite as determined from lattice vibrations. Contributions to Mineralogy and Petrology, 79, 56–76.

Salje, E., and Werneke, C. (1982b) How to determine phase stabilities from lattice vibrations. In W. Schreyer, Ed., High pressure researches in geoscience. E. Schweitzerbart'sche Verlagsbuchhandlung, Stuttgart, Germany.

Sanders, M.J., Leslie, M., and Catlow, C.R.A. (1984) Interatomic potentials for SiO_2. Journal of the Chemical Society, Chemical Communications, 1271–1273.

Saul, P., Catlow, C.R.A., and Kendrick, J. (1985) Theoretical studies of protons in sodium hydroxide. Philosophical Magazine B, 51, 107–117.

Vaughan, M.T., and Weidner, D.J. (1978) The relationship of elasticity and crystal structure in andalusite and sillimanite. Physics and Chemistry of Minerals, 3, 133–144.

Winkler, B., and Buehrer, W. (1990) The lattice dynamics of andalusite: Prediction and experiment. Physics and Chemistry of Minerals, 17, 453–461.

Winkler, B., Langer, K., and Johannsen, P.G. (1989) The influence of pressure on the OH valence vibration of zoisite. Physics and Chemistry of Minerals, 16, 668–671.

Winter, J.K., and Ghose, S. (1979) Thermal expansion and high temperature crystal chemistry of the Al_2SiO_5 polymorphs. American Mineralogist, 64, 573–586.

Manuscript received March 5, 1990
Manuscript accepted December 20, 1990